2014-01-0584
Published 04/01/2014

doi:10.4271/2014-01-0584
saepcmech.saejournals.org

Low Drag Automotive Mirrors Using Passive Jet Flow Control

Jianlei Wang
Northwestern Polytechnical Univ.

William Bartow, Andres Moreyra, Gregory Woyczynski, Alexis Lefebvre, Edward Carrington, and Gecheng Zha
University of Miami

1. ABSTRACT

This paper introduces and proves a novel automotive mirror base drag reduction method using passive jet flow control. The new concept is to open an inlet at the front part of the mirror, introduces the airflow via a converging duct, and ejects the jet surrounding the mirror surface at an angle toward the center of the mirror. The jet harnesses the energy from the free stream by jet mixing with the main flow via large coherent structures, entrains the main flow to energize the base flow, reduces the wake size and turbulence fluctuation, and ultimately significantly decreases the drag. Above phenomena are proved by wind tunnel testing with PIV and drag force measurement and CFD large eddy simulation (LES) calculation. Two jet mirrors with different inlet areas are studied. The jet mirror tunnel 1 has a smaller inlet area, and the jet mirror tunnel 2 has a 4.7 times larger inlet area. The wind tunnel testing is only done for the baseline and jet mirror tunnel 1. LES is used to study all the three mirror configurations. Both the wind tunnel testing and LES indicate that the jet mirror tunnel 1 reduces the drag by about 18% with smaller wake width. The LES indicates that the jet mirror tunnel 2 with larger inlet area further reduces the wake and achieves a drag reduction of 39%. This paper is only for proof of the concept and no design optimization is done. It is believed that there is a large room to further reduce the drag with a systematic design optimization.

CITATION: Wang, J., Bartow, W., Moreyra, A., Woyczynski, G. et al., "Low Drag Automotive Mirrors Using Passive Jet Flow Control," *SAE Int. J. Passeng. Cars - Mech. Syst.* 7(2):2014, doi:10.4271/2014-01-0584.

2. INTRODUCTION

With the increasing public concern on the global environment, reducing fuel consumption and emission pollution becomes more and more pressing. Automotive vehicles consuming fossil fuel is one of the major sources of greenhouse gas emission. Small and light cars become popular for their low fuel consumption. The appearance of electric cars is the consequence of this global trend to push clean technology. Due to the low power density of the current battery technology, the electric cars also tend to be made with small size and weight. With the decreasing car size and weight, wind noise becomes more annoying for the people inside the vehicle. Listening high resolution music on highway driving becomes more difficult. For heavy load trucks of long distance transportation, fossil fuel may remain as the major energy source in a foreseeable future due to its high energy density.

The aerodynamic drag is the major resistance that the propulsion system of a vehicle needs to overcome by consuming energy. Road vehicles in general have high drag coefficient due to bluff body shapes, which create high pressure drag due to base flow [1]. The flow pressure and momentum in the base region is very low because the flow suffers very high energy loss attributed to the abrupt cut off the solid wall surface. Vortex shedding, high turbulence intensity, high velocity fluctuation, and low total pressure are the typical features of base flows.

Drag reduction techniques for bluff bodies hence have their crucial significance for reducing automotive vehicle fuel consumption. Burestietal[2] gave a thorough review of bluff body drag reduction methods and their applications to heavy trucks. The often used drag reduction methods include boat-tailing [3], base bleed [4, 5], etc. The boat-tailing has been used in truck drag reductions inceit is relatively easier to implement [6], but it does increase the length, which has the limitation from both practical use and traffic regulations. The base bleed concept is typically used to introduce flow from the front stagnation region where the pressure is high, and to exit at the base center. The bleed will introduce a vortex in a counter-rotating direction of the original base vortex to break the focused vortices, increase the base pressure and reduce the pressure drag. However, few devices permit opening a hole at the center of the base without affecting the functions.

This paper is to demonstrate a novel based rag reduction method using passive flow control jet, which is invented recently by Zha [7, 8, 9] to reduce automotive mirror drag and noise. Hereafter, this new mirror concept will be termed as “Jet Mirror” for simplicity. The external rearview mirrors create 2-7% total drag of a typical car [10], and is more for heavy trucks. Such a drag contribution far exceeds the small mirrors area percentage in a car. Furthermore, the vortex shedding and turbulence fluctuation of the mirror base flow is also a serious noise source affecting the comfort of the driver and passengers. Fig.1 is a typical flow structure of a conventional car rear view mirror showing the vortex shedding flow structure. The front curvature is beneficial to reduce front stagnation pressure area and thus pressure drag, which is the so called “wing mirror”.

External rear view mirrors are required by legal regulations [11] as a safety device. Many efforts are made to understand the flows around mirrors and to reduce the mirror drag. For example, Olsson [12] did a series of trade studies using CFD and wind tunnel testing to investigate the effect of different mirror parameters, ultimately to achieve a design with minimum drag.

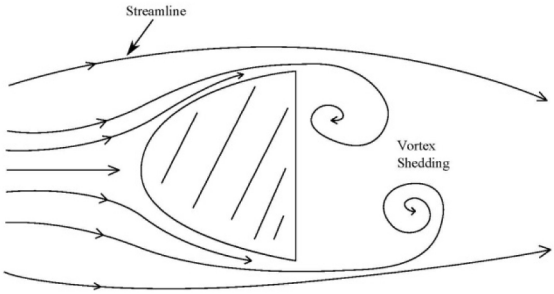

Fig. 1. Vortex shedding flow structure of a conventional car rear view mirror with wide wake.

3. JET MIRROR: THE NOVEL MIRROR CONCEPT

This new concept mirror using jet flow control [7, 8, 9] is aimed at substantially reducing the drag and noise of the conventional mirrors by using a passive flow control technique similar to those used for high lift slotted airfoil of aircraft.

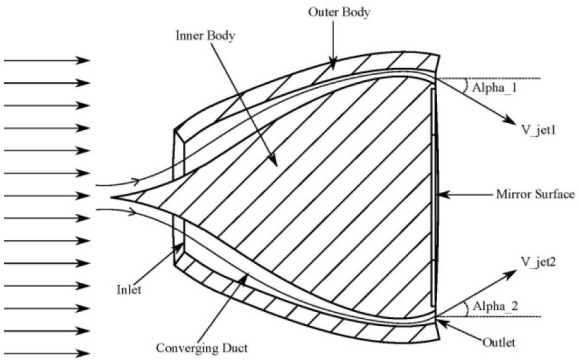

Fig. 2. A cross section sketch showing the configuration of a jet mirror.

Fig. 2 is across section sketch showing the configuration of a jet mirror and the expected flow structure. The jet is accelerated by the converging duct and by the low base pressure at the exit, where the main flow is at the highest speed and lowest pressure right before the separation due to the abrupt base geometry cut off.

The inlet size decides the amount of the air mass flow to be captured. The inlet can be any shape such as elliptic or rectangular that best matches the overall mirror configuration. Similarly, the mirror surface can be in any shape such as rectangular, elliptic, or round, etc.

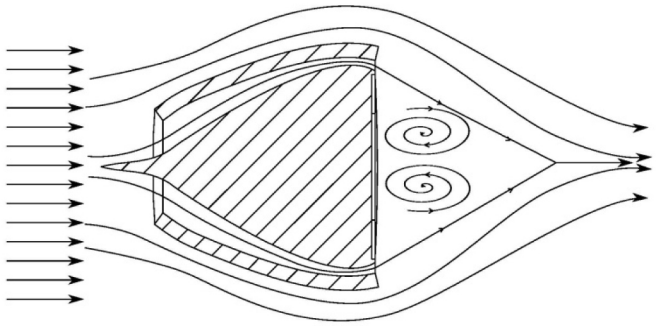

Fig. 3. The hypothesized flow structure with the virtual “trailing edge” and narrower wake

Working Mechanism: The aerodynamic jet mirror working mechanism is the following [7, 8, 9]:

1. The jet harnesses the high kinetic energy by capturing a large amount of free stream flow with a large opened inlet in the front. It renders the jet to exit the surrounding of the mirror base with high kinetic energy and high total pressure.
2. The high energy jet creates a mixing with the main flow with large vortex structures, which entrain the main flow to the base flow and energize the base flow.
3. The angled jet toward the mirror center induces the flow to form a virtual “trailing edge” as illustrated in Fig. 3, creates a more stable vortex zone behind the mirror, mitigates the vortex shedding and turbulence fluctuation, and reduces the wake size. It is well known that the aerodynamic drag is directly determined by the wake width. The smaller the wake, the smaller the drag.
4. The energized base flow and shrunk wake size increase base static pressure. The opened inlet reduces the front blockage by passing the flow and decrease the front area stagnation pressure area. These effects result in the reduced pressure drag. The reduced vortex shedding and turbulence fluctuation yields lower turbulence mixing noise that discomforts the driver and passengers.

To further reduce the base drag, the jet mirror can combine the base bleed technique by replacing the center body nose tip with an opened duct all the way to the mirror surface. The disadvantage of this combined configuration is that it will block a little visibility of the mirror due to the hole in the mirror center.

If the duct is designed to have no flow separation, the geometry parameters important to determine the wake and vortex shedding mitigation include: 1) Inlet area; 2) area ratio of the inlet to outlet; 3) exit jet slot angle.

The inlet area determines how much mass flow will be captured to form the jet. The more mass flow, the higher momentum of the exit jet will have. The area ratio of the inlet to jet exit will determine the jet velocity. The higher the ratio, the smaller the jet exit area, and hence the higher the jet velocity. The exit jet slot angle is to guide the jet direction α as indicated in Fig. 2. The jet momentum, velocity and jet direction determined by these parameters are expected to have a strong influence on the jet mixing pattern, even though the specific effect from each parameter is not known yet at this time.

4. RESEARCH APPROACHES

The approaches used in this paper to demonstrate the advantages of the mirror include Large Eddy Simulation (LES) using a computational fluid dynamics (CFD) program and wind tunnel testing. This paper only studies a baseline mirror and two jet mirrors with no optimization. The purpose is only to demonstrate the concept. Design optimization and refinement will be the future work.

4.1 Wind Tunnel Testing

4.1.1 Flow Visualization

All aerodynamic flow visualization and PIV velocity field measurement were acquired at the University of Miami 24″×24″wind tunnel facilities at a rate of 50 samples per second. Since the drags of the tested mirrors are too small and are within the uncertainty of the wind tunnel force balance, accurate drag measurement cannot be obtained with this wind tunnel facility and is conducted separately.

A LaVision Digital Particle Image Velocimetry (DPIV) system with a Litron Nano Nd:YAG 200 mJ/pulse was used to monitor and acquire the velocity field surrounding the airfoil. An adaptive 64×64 to 32×32 pixel cross-correlation analysis method was used with masking over the airfoil, resulting in 75×100 total vectors (including the airfoil). A series of 1,000 velocity fields were acquired for each case. The accuracy of PIV measurements ultimately depends on the uncertainty of the measurements of particle displacement. For standard 2D cross-correlation-based sub-pixel PIV processing techniques, the commonly accepted uncertainty in the displacement measurement is 0.1 pixels. Based on the current measurement scale (6.7pix/mm) and time interval between two exposures (10μs), the instantaneous velocity measurement uncertainty is estimated to vary within 2.8%. A customized flow seeder using the same particles for PIV tracers was used for flow visualization. All the results presented were acquired at the mid-span plane section.

4.1.2 Drag Force Measurement

The force measurement experiment is performed in an open-jet closed circuit low speed wind tunnel at North Western Polytecnical University in Xian, China. The test section is circular with a diameter of 1.5m. The maximum velocity of the wind tunnel is 45m/s without any model. The turbulivity of the wind tunnel is lower than 0.02%. The mirror model is tested at free stream velocity from 15m/s to 40m/s with a Reynolds number from 1.4×10^5 to 3.6×10^5 based on the length of the mirror.

The maximum scale of the force balance in the drag direction is 80N and the accuracy of the balance is 0.02% of the full scale. In this test we acquire data at the frequency of 100 KHz and the results are averaged with 30 seconds testing time.

4.2 Large Eddy Simulation

The in house high order accuracy CFD code FASIP, which is intensively validated with various 2D and 3D steady and unsteady flows, is used for the LES analysis [13, 14, 15]. High order shock capturing schemes, including 3rd order MUSCL scheme, 3rd, 5th and 7th order WENO schemes and a finite compact scheme combining a shock detector and 6th order Pade scheme, are utilized in the code. A set of 4th order and 6th order central differencing schemes are devised to match the same stencil width of the WENO schemes for the viscous terms. The Roe's scheme and a low diffusion E-CUSP scheme developed by Zha et al are used as the approximate Riemann solver with the MUSCL and WENO shock capturing schemes. For turbulent simulations, FASIP has implemented Detached Eddy Simulation (DES), Large Eddy Simulation (LES) [14, 15], and Reynolds averaged Navier-Stokes (RANS). An implicit 2nd order time accurate scheme with pseudo time and unfactored Gauss-Seidel line relaxation is employed for time marching. For aero elasticity problems, a fully coupled fluid-structural interaction model is implemented. The MPI parallel computing is utilized and a high scalability is achieved.

5. PROTOTYPE MODELS

A baseline mirror shape is created similar to a Mini-Cooper mirror as shown in Fig. 4. However, an actual car mirror usually has a cavity effect due to the recessed position of the mirror relative to the mirror house aft edge. Such a cavity effect is known to have some drag reduction effect and is not simulated in this study. In other words, the mirror surface of the prototype is located right at the very aft position.

Three prototype models configurations are studied in this paper, namely, the baseline mirror, tunnel 1 jet mirror, tunnel 2 jet mirror. Fig. 5 displays the baseline (a) and tunnel 1(b) geometry. All the three prototypes have the same outer casing shape and size. The maximum section area is located at the mirror surface and is an ellipse with an area of $18884mm^2$.

The tunnel 2 has an inlet area 4.7 times greater than the tunnel 1. It is hence expected that the tunnel 2 will have higher jet momentum and velocity. The tunnel 2 also has an enlarged exit flow area that is 2.65 times greater than that of tunnel 1. Both tunnels have an exit duct angle of 7°.

For the wind tunnel testing, only the baseline mirror and the jet mirror tunnel 1 model are tested as shown in Fig. 6a and 6b, which are the photos of the models attached in the wind tunnel. For the LES, all the three models are simulated. Figure 7 presents the coordinate system of the model used in both the numerical simulation and wind tunnel test.

Fig. 4. Mini Cooper mirror

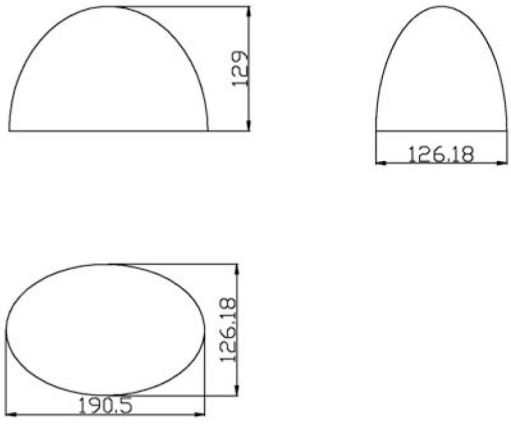

(a). Baseline model

Fig. 5.

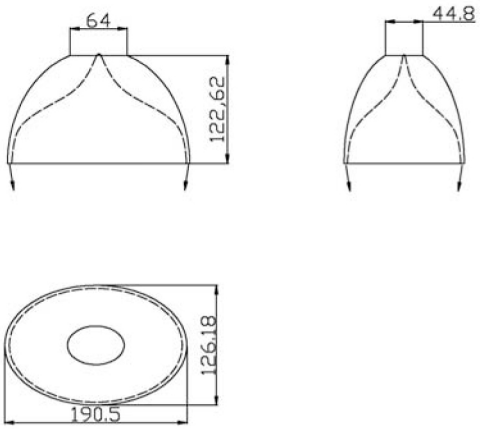

(b). Tunnel 1 model

Fig. 5. (cont.) Test model

(a). Baseline mirror model

(b). Tunnel 1 Jet mirror model

Fig. 6. Mirror model tested in wind tunnel.

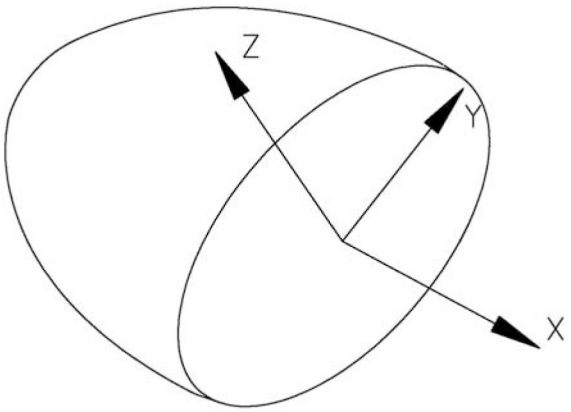

Fig. 7. Model coordinates

6. RESULTS AND DISCUSSION

6.1 Wind Tunnel Testing Results

6.1.1 PIV and Flow Visualization

For the wind tunnel testing, only the baseline and tunnel 1 configurations are measured. The results presented have the free stream velocity U_∞ = 30m/s with a Reynolds number 2.75×10^5 based on the length of the mirror. The PIV measurement plane is at the mid-cross section. Fig. 8 shows the PIV setup.

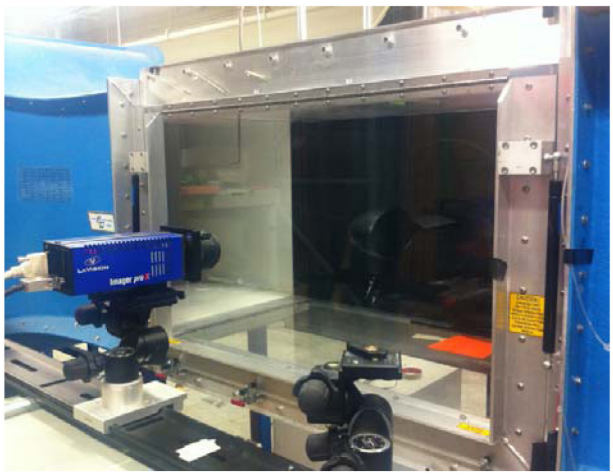

Fig.8. PIV setup

Figure 9 shows the time averaged2D velocity field measured by the PIV at the mid-section for the baseline and tunnel 1. X and Z coordinates are normalized by the length of the short axis of the mirror section (X=0 section Y direction). The velocity is normalized by the free stream velocity.

Fig. 9 shows that both the baseline mirror and the jet mirror tunnel 1 have vortex shedding, reflected as two counter rotating vortices of the averaged velocity field. The averaged PIV results show that the wake area of tunnel 1 clearly has a converging shape and is narrower than the wake of baseline as expected. The two vortices of the baseline mirror are further apart and the two vortices of the jet mirror tunnel 1 are closer to each other due to the reduced wake width.

Figure 10 shows the instantaneous flow visualization at mid-plane (Y=0) section, which indicates again that the wake of the baseline mirror (Fig. 10 a) is wider and has an open end, whereas the wake of the tunnel 1 (Fig. 10 b) is clearly converging after the mirror surface. This proves the hypothesis that the jet mirror has a narrower wake.

Fig. 11 compares the instantaneous PIV results of the baseline mirror and jet mirror tunnel 1. At that instant, the baseline mirror has two stronger vortices, whereas the jet mirror's vortices are not clear and appears to be weaker. The high speed envelop of the wake of the jet mirror tunnel 1 is clearly showing a converging shape than the baseline mirror, consistent with the observation in Fig. 9 and 10.

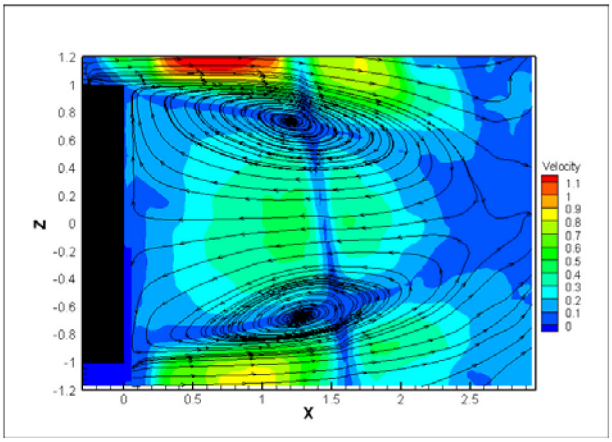

(a). Baseline

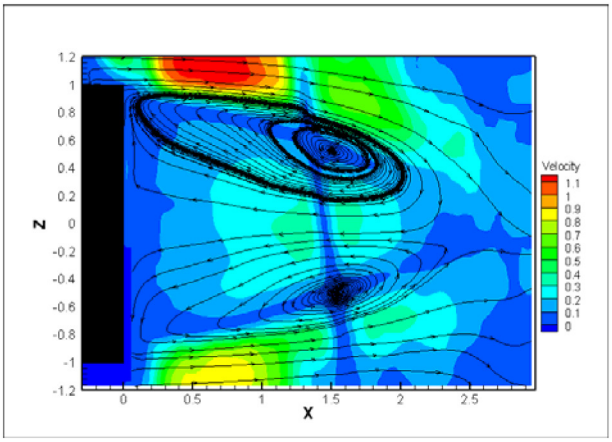

(b). Tunnel 1

Fig. 9. Averaged PIV results, 30m/s

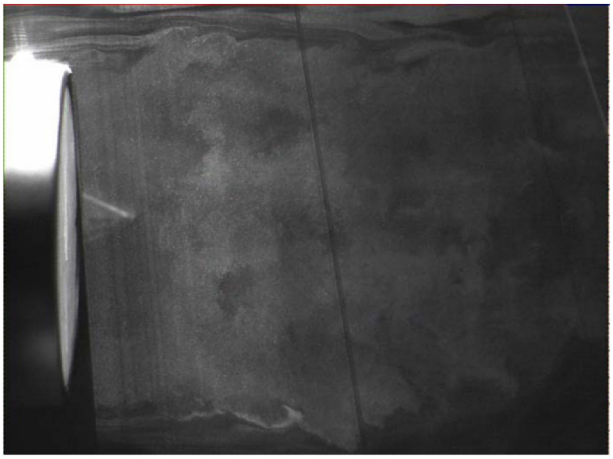

a). Baseline

(b). Tunnel 1

Fig. 10. Instantaneous flow visualization, 30m/s

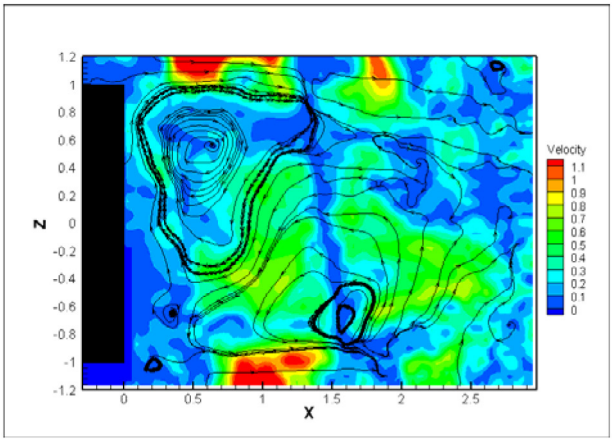

(a). Baseline

Fig. 11.

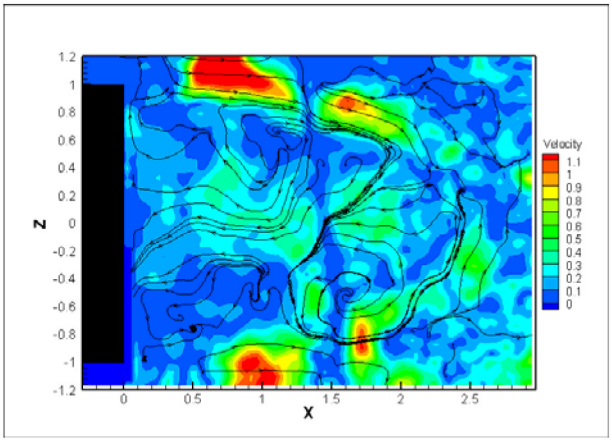

(b). Tunnel 1

Fig. 11. (cont.) Instantaneous PIV velocity fields, 30m/s

Figure 12 shows the zoomed flow visualization near the jet region at the mid-cross section (Y=0 section). It can be seen that the jet is sucked upward by the mainstream even though the jet has an angle toward the center axis of the mirror. The jet mixing with the main flow creates clear large coherent vortex structures, which entrain the main flow to the base flow and energize it. The overall effect is that the wake boundary is brought toward the center and the wake becomes narrower. This indeed indicates that the jet mirror works as hypothesized.

Fig. 12. Zoomed jet area of the jet mirror (tunnel 1) showing large coherent vortex structures.

6.1.2 Drag Force Measurement

For the drag force measurement in the open wind tunnel, the test model is mounted at one end of the balance as shown in Fig. 13a, which is the baseline model. To protect the balance, an aluminum cover is mounted at the model end of the balance. Fig. 13b is the model of the jet mirror tunnel 1.

Table 1 is the measured drag of the baseline mirror and the jet mirror tunnel 1 at the free stream velocity from 15m/s to 40m/s. The averaged drag reduction is about 18%.

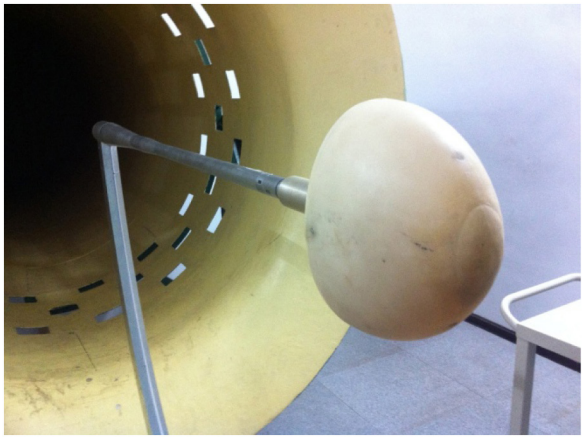

(a). Baseline model

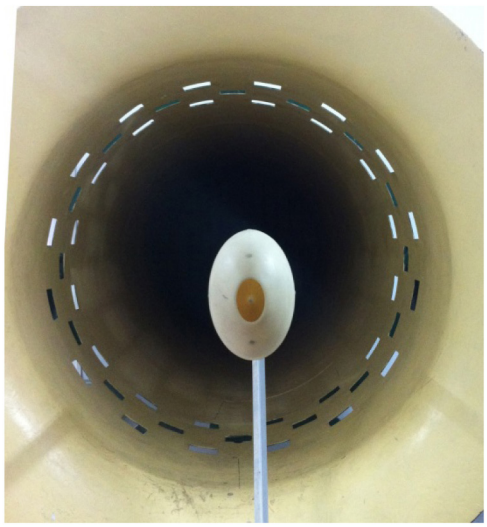

(b). Tunnel 1 model

Fig. 13. Test model in the wind tunnel

Table 1. Measured drag for baseline and jet mirror tunnel_1

V, m/s	Drag(N)		Cd		Drag reduction(%)
	Baseline	Tunnel_1	Baseline	Tunnel_1	
15	0.8	0.7	0.33	0.26	18.65
22	1.7	1.4	0.31	0.25	19.20
25	2.2	1.7	0.31	0.25	20.11
30	3	2.5	0.31	0.25	17.94
35	4.1	3.4	0.30	0.25	16.68
40	5.2	4.4	0.30	0.25	16.68

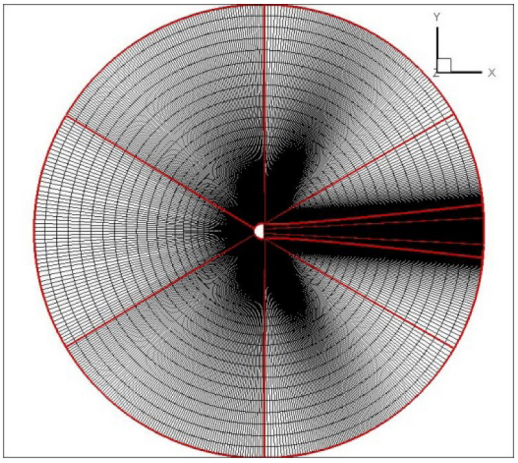

(a). Mid-cross section mesh

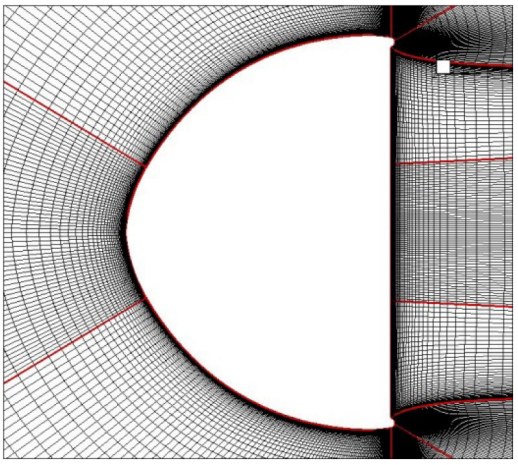

(b). Zoomed mid-cross section mesh

Fig. 14. Mesh for the baseline mirror.

6.2 Large Eddy Simulation Results

The Mach number and Reynolds number used in the numerical simulation is 0.088 and 2.27×10^5 respectively, same as the parameters used in the wind tunnel test. The implicit LES methodology used by Shen and Zha in [21] is adopted. The Roe scheme is used with the 3rd order WENO scheme for the in viscid fluxes. Second order differencing is used for the viscous terms. The normalized physical time step of 0.02 is used.

6.2.1 Mesh

Structured meshes are used in all the three cases. The mesh sizes are about6×10^6 for baseline and 3×10^6 for tunnel 1 and tunnel 2.Fig. 14, 15, 16 show the mesh topology of the mid-cross section. The far field boundary of the mesh is located at 20 times length of the mirror away from the model. Fig. 14 is the mesh for the baseline mirror with no jet flow control. Fig. 15 is the jet mirror with tunnel 1 geometry. Fig. 16 is the jet mirror with tunnel 2 geometry, which shows that the tunnel 2 with a 4.7 times larger inlet area than the tunnel 1 configuration.

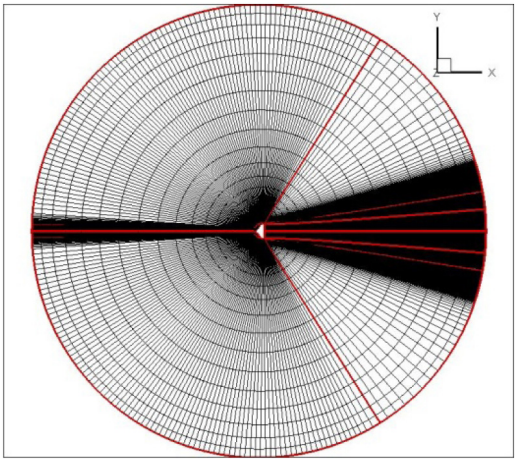

(a). Mid-cross section mesh

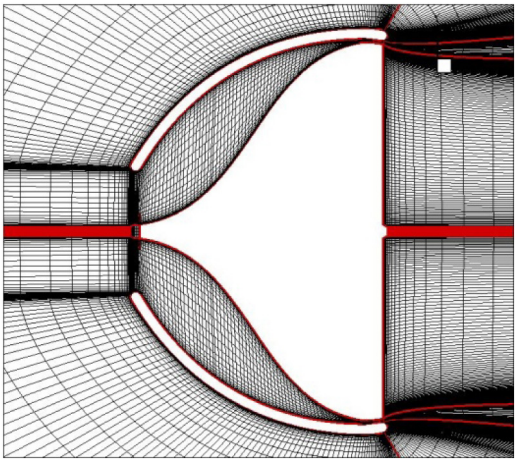

(b). Zoomed mid-cross section mesh

Fig. 15. Mesh for the jet mirror, Tunnel 1.

6.2.2 Drag Coefficient

Fig. 17 shows the time history of the computed drag coefficient of jet tunnel 5, which indicates the drag fluctuation due to vortex shedding. Table 2 shows the time averaged drag coefficient results. The baseline mirror has the predicted drag coefficient of 0.46, which is significantly higher than the 0.3 measured in the wind tunnel as shown in Table 1. The drag coefficient of the jet mirror tunnel 1 is predicted to be 0.38, also significantly higher than the measured one. The reason why the value predicted by CFD has a significant discrepancy from the experiment is not clear and will be is investigated from both the wind tunnel measurement and CFD mesh refinement.

However, the predicted drag reduction amount of 17.4% matches very well with the experimental measurement of 17.94% at the same velocity, 30m/s. The predicted drag reduction of the tunnel 2 is 39.1%, which is radical. Please note that there is not any optimization done for the present configurations, which are created only for the purpose of proof of concept. It is expected that there is a large room to further improve the drag reduction.

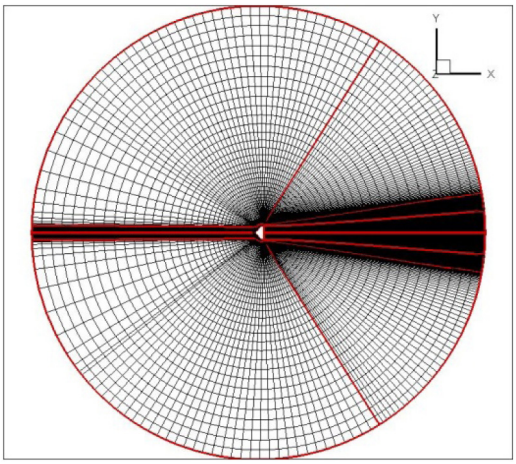

(a). Mid-cross section mesh

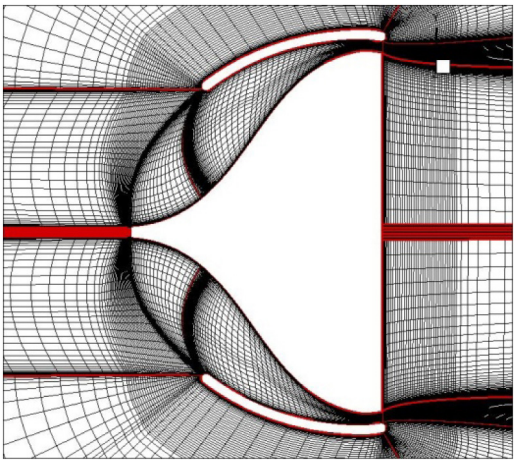

(b). Zoomed mid-cross section mesh

Fig. 16. Mesh for the jet mirror, Tunnel 2.

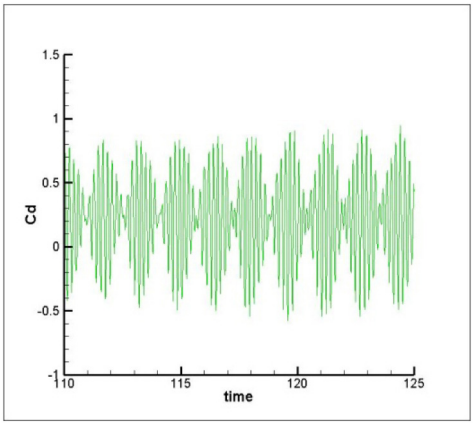

Fig. 17. Drag coefficient time history

6.2.3 Flow Field

Fig. 18 shows the instantaneous Mach number at the semi-minor axis plane section (y=0 section). The wake width of the jet mirror tunnel 1 and 2 are significantly reduced compared with the baseline mirror. The wake of tunnel 2 is the narrowest of the three due to the stronger jet momentum. In the jet region, it can be seen that the jet mirror tunnel 2 has higher jet velocity than the tunnel 1 due to greater captured mass flow rate.

Table 2. Drag coefficient results.

Mirror	Cd, Drags Coefficient	Drag Reduction
Baseline	0.46	
Tunnel 1	0.38	17.4%
Tunnel 2	0.28	39.1%

Fig. 19 is the zoomed instantaneous Mach number contours at the cross section corner region to compare the baseline and jet mirror flow fields. The baseline mirror flow (Fig. 19a) reaches the maximum speed at the base edge and a low speed base flow is formed at the base due to the flow separation. Fig. 18b shows that for the tunnel 1, the jet flow reaches the maximum speed at the jet exit and is sucked upward to merge with the main flow since the jet has higher static and total pressure. This phenomenon matches excellently with the experimental visualization shown in Fig. 12. However, the CFD has not captured the coherent vortex structure. It may be because the mesh needs to be much more refined in the jet mixing region.

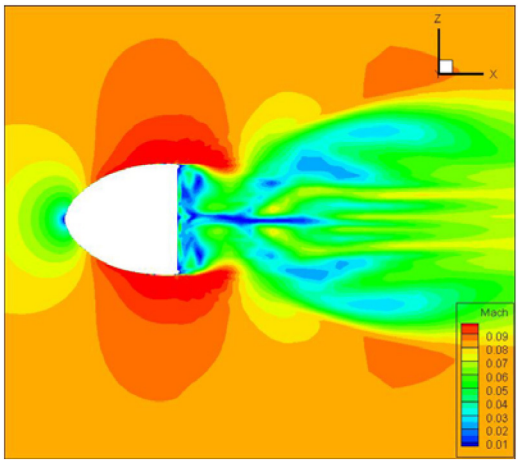

(a). Baseline

Fig.18.

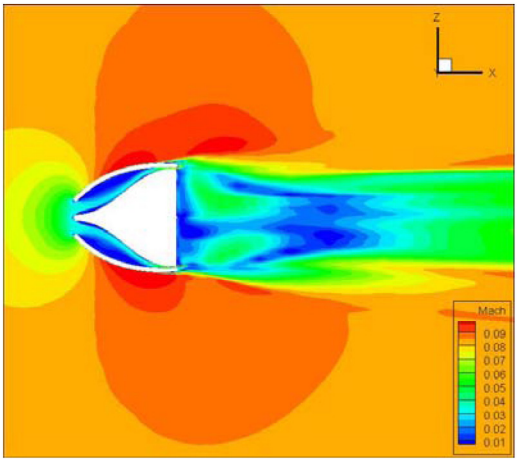

(b). Tunnel1

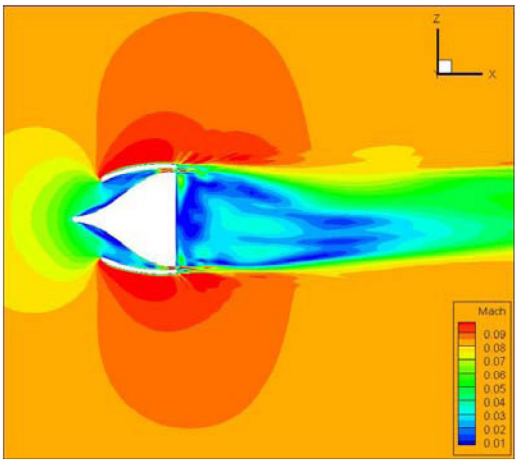

(c). Tunnel 2

Fig.18. (cont.) Mid-section Mach contours

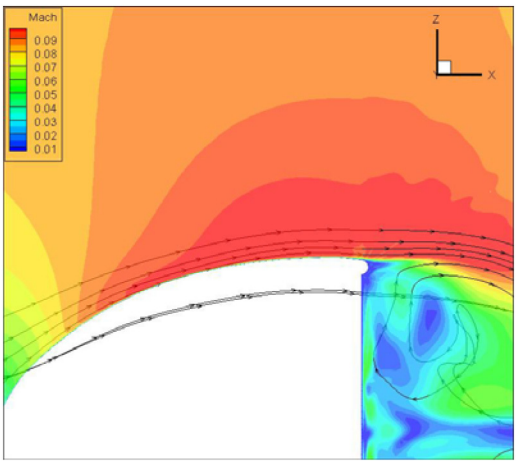

(a). Baseline

Fig. 19. Mid-section Mach contours

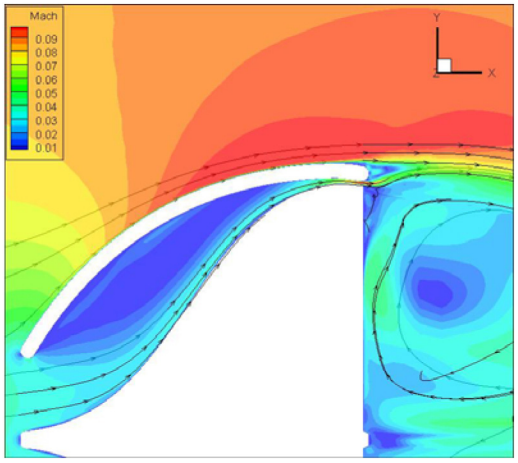

(b). Tunnel 1

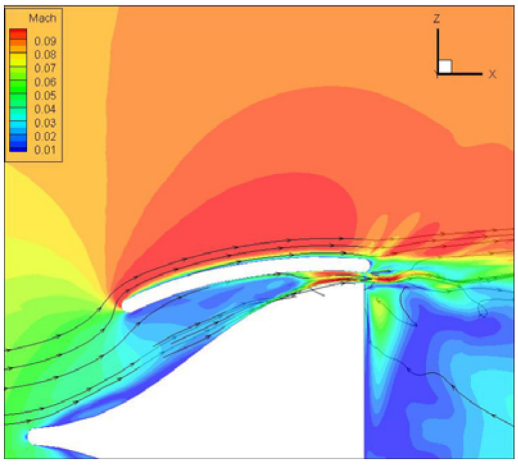

(c). Tunnel 2

Fig. 19. (cont.) Mid-section Mach contours

Fig. 19c shows that the jet is stronger with higher exit speed for tunnel 2 since the inlet area is 4 times greater than that of tunnel 1. The jet is also sucked upward and shows the trend of coherent vortex structure with curved streamlines. More post-processing of the LES results will be presented in the final paper.

To see the energy loss of the wake and base flow, Fig. 20 displays the entropy contours at the constant axial location one mirror length downstream of the mirror surface. It can be seen that the baseline mirror has a much larger high entropy area than the other two jet mirrors. The jet mirror tunnel 1 significantly reduces the entropy footprint from the baseline mirror. By increasing the inlet area, the jet mirror tunnel 2 has further shrunk the entropy footprint. This is consistent with the drag values given in Table 2 that the jet mirror tunnel 1 has smaller drag than the baseline mirror, and the jet mirror tunnel 2 has smaller drag than tunnel 1.

Ultimately, for drag reduction, what is of interest is the surface pressure to examine if the pressure drag is reduced. Fig. 21a and b are the surface pressure contours with streamlines colored by Mach number contours. Fig. 21a shows that the baseline mirror has a large high pressure area in the front due to the stagnation region. At the mirror base area, the pressure is lower and is fairly uniform. There are vortices near the mirror surface with low speed (blue color streamlines). The wake boundary streamlines have high speed with red color and the wake shape is fairly open ended consistent with the experimental observation in Fig. 10.

Fig. 21b shows that the base mirror surface has an area of high pressure (red color), which will contribute to pressure drag reduction. The wake boundary streamlines are much more converged than the baseline mirror. It is the desired virtual “trailing edge” or “boat tail”. It results in narrower wake and smaller drag.

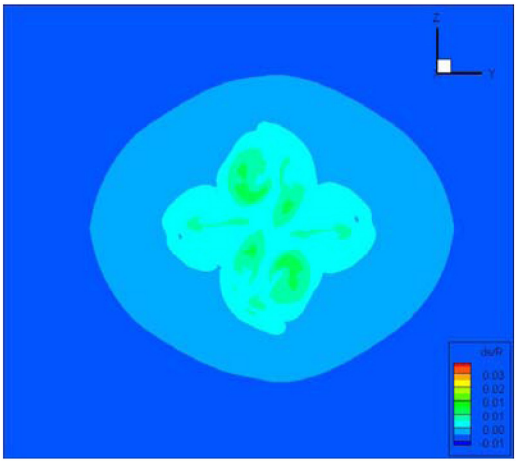

(a). Baseline mirror

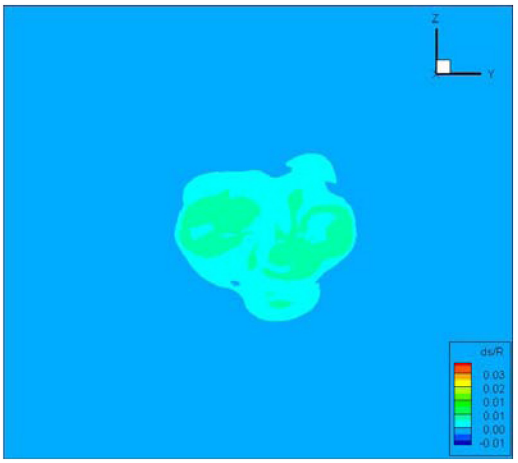

(b). Jet mirror, tunnel 1

Fig. 20. Entropy contours at one-mirror length downstream of the mirror

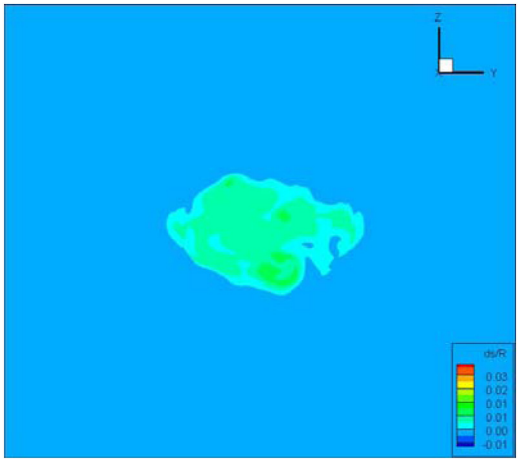

(c). Jet mirror, tunnel 2

Fig. 20. (cont.) Entropy contours at one-mirror length downstream of the mirror

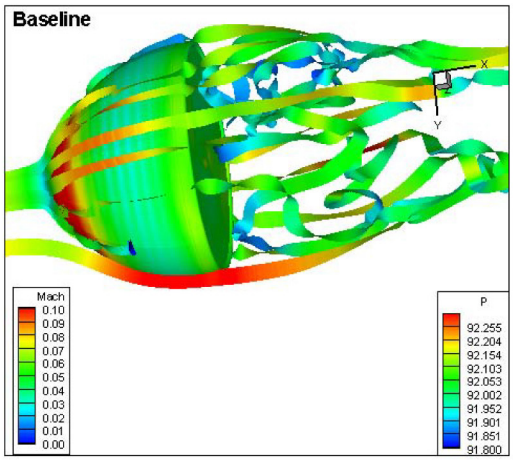

(a) Baseline mirror

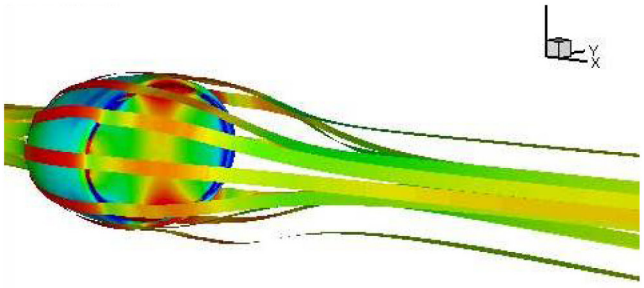

(b) Tunnel 2

Fig. 21. Surface pressure contours with streamlines colored by Mach number

7. CONCLUSIONS

The novel drag reduction method for automotive mirrors using passive jet flow control suggested by Zha is demonstrated to be very effective by both wind tunnel testing and LES. Two jet mirrors with different inlet areas are studied. The jet mirror tunnel 1 has a smaller inlet area, and the jet mirror tunnel 2 has a 4.7 times larger inlet area. The wind tunnel testing is only done for the baseline and jet mirror tunnel 1. LES is used to study all the three mirror configurations. The LES predicted drag value is significantly higher than the experimental measurement. However, the drag reduction predicted by the LES agrees excellently with the experiment. Both the wind tunnel testing and LES indicate that the jet mirror tunnel 1 reduces the drag by about 18% with smaller wake width. The LES indicates that the jet mirror tunnel 2 with larger inlet area further reduces the wake and achieves a drag reduction of 39%. The wind tunnel flow visualization and PIV show that the jet from the mirror is sucked upward due to the high total pressure of the jet. The jet mixing with the main flow creates large coherent vortex structures, which entrains the main flow to the base flow, energizes the base flow, reduce wake size, turbulence fluctuation, and ultimately reduce drag and noise. The noise reduction hypothesis is not studied in this research and will be investigated in future.

REFERENCES

1. Hucho, W.-H. and Sovran, G., “Aerodynamics of Road,” Annual Review of Fluid Mechanics, vol.25, pp.485-537, 1993.
2. Buresti, G. and Iungo, G.V. and Lombardi, G., “Methods for The Drag Reduction of Bluff Bodies and Their Application to Heavy Road-Vehicles.” 1st Interim Report Contract between CRF and DIA, DDIA2007-6, Oct.2007.
3. Maull, D.J. and Hoole B.J., “The effect of boat-tailing on the flow around a two-dimensional blunt-based aero foilat zero incidence,” J.Royal Aero. Soc., vol.71, pp.854-858, 1967.
4. Berman, P.W., “Investig a tionin to the effect of base bleed on the flow behind a two-dimensional model with a blunt trailing edge.” AGARDCP-4, Part2, pp.485-507, 1966.
5. Falchi, M. and Provenzano, G. and Pietrogiacomi, D., “Experimental and numerical investigation of flow control on bluff bodies by passive ventilation,” Experiments in Fluids, vol.41, pp.21-33, 2006.
6. McCallen, R., “DOEs Effort to reduce truck aerodynamic drag through joint experiments and computations.” Presentation at the DOE Heavy Vehicle Systems Optimization Merit Reviewand Peer Evaluation, Argonne National Laboratory, April18-20, 2006.
7. Zha, G.-C., “Low Noise and Low Drag Automobile Mirrors Using Jet Flow Control”, UMM-115, University of Miami Invention Disclosure, Sept.7, 2012.
8. Zha, G.-C., “Low Noise Low Drag Auto mobile Mirrors,” Provisional Patent filed to USPTO, 61/765, 219,02/15/2013, 2013.
9. Zha, G.-C., “Low Drag Low Noise Automobile Mirrors Using Jet Flow Control,” Patent Corporation Treaty, PCT/US2013/053191, filed to USPTO, 08/01/2013, 2013.
10. Hucho W. H.. Aerodynamik des Automobils. Wieweg Teubner, fifth edition, 2005.
11. EUR Lex Access to European Union law. Directive 2003/97/EC. http://eurlex.europa.eu/LexUriServ/LexUriServ.do?uri=CELEX:32003L0097:en:NOT, 2011.
12. Olsson, M., “Designing and Optimizing View Mirrors.” Master Thesis, Chalmers University of Technology, Goteborg, Sweden, 2011.
13. Shen, Y.-Q. and Zha, G.-C. and Chen, X.-Y., “High Order Conservative Differencing for Viscous Terms and the Application to Vortex-Induced Vibration Flows,” Journal of Computational Physics, vol.228(2), pp.8283-8300, 2009.
14. Shen Y.-Q. and Zha G.-C., “Large Eddy Simulation Using a New Set of Sixth Order Schemes for Compressible Viscous Terms,” Journal of Computational Physics, vol.229, pp.8296-8312, 2010.
15. Im, H-S., Zha, G-C., Dano B. P. E. “Large Eddy Simulation of Coflow Jet Airfoil atHigh Angle of Attack” J. of Fluids Engineering, FEB. 2014, Vol. 136 / 021101-1.